

# Weld Microstructure Development and Properties of Precipitation-Strengthened Martensitic Stainless Steels

*The cracking behavior and mechanical properties are discussed in terms of microstructural evolution*

BY J. A. BROOKS AND W. M. GARRISON, Jr.

**ABSTRACT.** The weld microstructural evolution, mechanical properties and solidification cracking susceptibility of three precipitation-strengthened martensitic stainless steels — PH 13-8 Mo, Custom 450 and 15-5 PH — were investigated. Liquid tin quenching of gas tungsten arc welds revealed that all three welds solidified as single-phase ferrite with a high degree of microsegregation. However, during further solidification and cooling almost complete homogenization occurred as a result of solid-state diffusion. The welds in all three alloys exhibited good resistance to solidification cracking and generally exhibited tensile and impact properties similar to those of the base metal. However, in almost all cases, the weld Charpy impact energies were somewhat less than those of the base metals. The cracking behavior and mechanical properties are discussed in terms of microstructural evolution.

## Introduction

The precipitation-strengthened martensitic stainless steels are used for their high strength, higher than that of the austenitic stainless steels, and good corrosion resistance, better than the hardenable 400 series stainless steels (Ref. 1). These alloys form a low-carbon martensite with  $M_s$  temperatures just above room temperature, and are precipitation strengthened by one or more of the following elements: Cu, Al, Ti, Nb and Mo (Refs. 2–4). In general, these materials exhibit good weldability; however, they exhibit an embrittlement coincident with the onset of precipitation hardening that

has precluded the use of some alloys of this type in applications requiring high toughness (Ref. 5).

Often, the evolution of the weld microstructure is not well understood or considered by the welding engineer or metallurgist. Rather, emphasis is directed at developing a defect-free weld that meets minimum property requirements. Although the engineering application is of primary importance, only by understanding the evolution of the microstructure can one expect to readily optimize welding processes and subsequent weld properties. The evolution of weld microstructures of these alloys has never been studied in detail. This investigation studies three such alloys: PH 13-8 Mo (USN S13800), strengthened by NiAl; 15-5 PH (USN S15500), strengthened by particles of elemental Cu; and Custom 450 (USN S45000), strengthened with particles of elemental Cu and possibly a Nb- and Mo-containing Laves phase. The solidification cracking susceptibility and weld tensile and impact properties were investigated and are discussed in terms of microstructural evolution revealed with the use of liquid tin quenching.

## Experimental

Compositions of the three martensitic stainless steels are shown in Table 1. All three alloys were from commercial heats. The VAR PH 13-8 was obtained from Armco and the ESR Custom 450 was obtained from Carpenter Technology. Both alloys were in the form of an 8-in. round corner square bar. The 15-5 PH was obtained from G. O. Carlson in the form of ½-in. plate. The PH 13-8 and Custom 450 were upset and cross forged at 1200°C (2192°F) to plate 0.6 and 0.4 in. thick, 14 in. wide and approximately 3 ft long. Smooth axisymmetric tensile properties and the Charpy impact energy were determined for both welds and base metals in the unaged condition and as a function of aging temperature. The mechanical properties of the base plates were obtained using specimens that were austenitized, oil quenched and then aged. Refrigeration to liquid nitrogen temperature subsequent to oil quenching and prior to aging had negligible effects on the strength and Charpy impact properties of Custom 450 and 15-5 PH when aged between 450 and 550°C (842–1022°F) for 1 h. Under the same conditions, the impact toughness of PH 13-8 was actually reduced ~20% when aged at 450°C and reduced ~30% when aged at 500°C, while the yield strength increased ~3 and 6%, respectively, as a result of refrigeration. When aged at 550°C, the properties were unaffected as a result of refrigeration prior to aging. Consequently, refrigeration was not used on any of the specimens in this study. Weld plates 6.4 x 30.5 cm (2.5 x 12 in.) were austenitized for 1 h and air cooled prior to welding. An austenitizing temperature of 927°C (1700°F) was used for PH 13-8 Mo while that for Custom 450 and 15-5 PH was 1038°C (1900°F).

Mechanical test specimens were cut from GTA cold wire feed welds with the

## KEY WORDS

Austenite  
Charpy Impact Energy  
Ferrite  
Microstructure  
Precipitation Hardening  
Solidification  
Tin Quenching  
Varestraint Testing

J. A. BROOKS is with Sandia National Laboratories, Livermore, Calif. W. R. GARRISON, Jr., is with Carnegie-Mellon University, Pittsburgh, Pa.

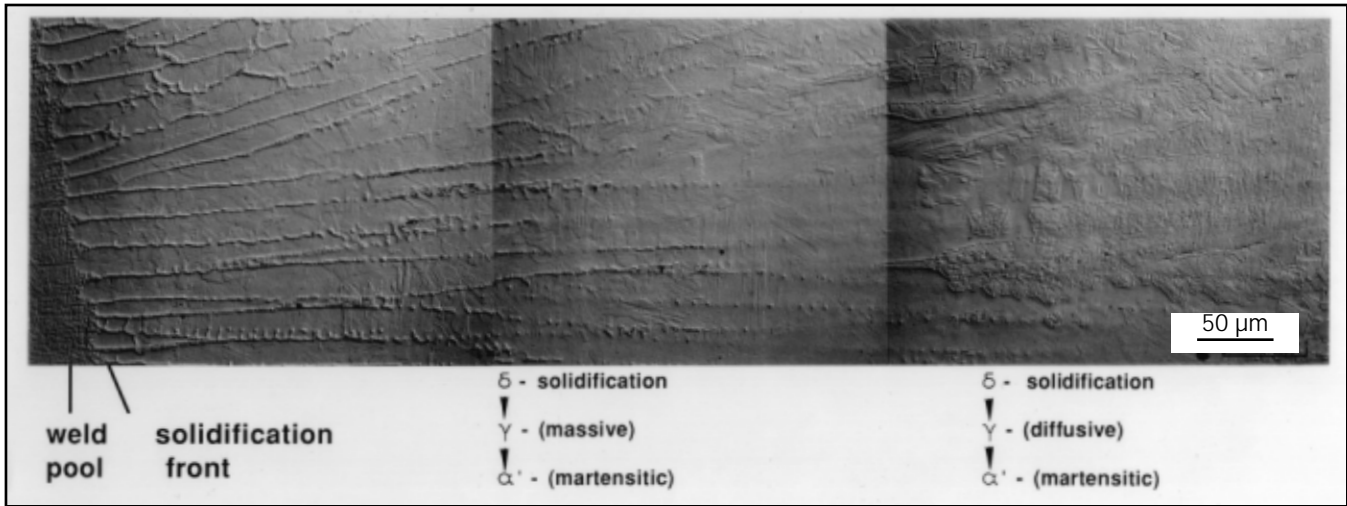


Fig. 1 — Montage of liquid tin-quenched Custom 450 GTA weld showing the evolution of the weld microstructure from the dendrite tips in the weld pool to the region of solid-state transformation of ferrite to austenite. Captions show sequence of transformations.

**Table 1 — Alloy Compositions (wt-%)**

Alloy	C	Cr	Ni	Cu	Al	Mo	Si	Mn	Nb	P	S	N
PH 13-8 Mo	0.03	12.63	7.9	—	1.08	1.73	0.04	0.05	—	0.005	0.005	0.002
Custom 450	0.03	14.75	6.44	1.5	—	0.76	0.4	0.33	0.75	0.008	0.005	0.035
15-5 PH	0.02	14.7	4.7	3.2	—	0.38	0.33	0.33	0.2	0.017	0.007	—
304L-F	0.017	19.1	10.7	—	—	0.21	0.54	1.9	—	0.24	0.001	0.035
304L-A	0.020	18.7	10.9	—	—	0.19	0.53	1.7	—	0.020	0.008	0.035

sample length transverse to the weld direction. The weld fusion zone was placed in the center of the specimens with the notch of the Charpy specimens at the weld root. Tensile specimens, 5 mm in diameter and 20 mm long (0.2 x 0.79 in.), contained a composite of the fusion zone (~50%), HAZ and base metal. The tensile specimens deformed uniformly when tested, indicating no one zone dominated the tensile response; specimens also fractured near the weld center. The nominal weld parameters and plate thicknesses corresponding to the test results are shown in Table 2. A U-groove joint preparation and 1.14-mm (0.045-in.) welding wire were used with an interpass temperature of ~65°C (~150°F) for both plate thicknesses.

The solidification cracking susceptibility was evaluated in the unaged condition using sub-size Varestraint testing (Ref. 6). For comparison, tests were conducted on two commercial vacuum-induction melted/vacuum-arc remelted heats of 304L (USN S30403): one that solidified as primary ferrite, designated 304L-F, and the other that solidified as primary austenite, designated 304L-A. The compositions of these two heats of 304L are shown in Table 1. Welding parameters used during Varestraint testing are given in Table 2.

Metallographic samples of tin quenched and Varestraint specimens

**Table 2 — Nominal Weld Parameters**

Samples	Thickness (in.)	Amps	Volts	Speed (in./min.)	Wire Feed (in./min.)	No. Passes
Varestraint	0.25	180	12	6.0	—	1
Tensile	0.375	200	10	6.0	20	14-16
Charpy	0.5	200	10	6.0	20	20-24

were prepared using standard metallographic techniques with the final polish made with a 0.05-micron silica aqueous solution. A Vilella's etch was used to reveal the microstructural features. Microprobe analysis for compositional determination was conducted using a Joel 8900 microprobe with a 1-micron beam size operated at 15 and 25 KEV, depending upon feature size, and a 25-nA beam current. Samples for TEM analysis were electropolished and examined on a Joel 200 CX microscope. Fracture surfaces of Charpy samples were examined using SEM.

### Microstructural Evolution

In this investigation, GTA welds were quenched with liquid tin during welding in an attempt to capture insitu the evolution of the weld microstructure from the first stages of solidification to that observed at room temperature. Figure 1

shows results from a Custom 450 weld obtained using this technique. The microstructure is evolving from left to right with the quenched weld pool and solidifying dendrite tips shown in the left side of the micrograph. Microsegregation occurring from elemental partitioning between the solid and liquid during weld solidification is evident in the interdendritic regions of the cellular/cellular-dendritic solidifying structure. However, it appears that homogenization occurs during further solidification and cooling (moving from left to right in the micrograph). At a lower temperature (in the right-hand side of the micrograph), the ferrite has started to transform to austenite by a diffusion-controlled process. When cooled below the  $M_s$  (in this case, assisted by the tin quenching), the austenite transforms to martensite. Thus, the total evolution of the weld microstructure can be observed in one micrograph.

Electron microprobe analysis was



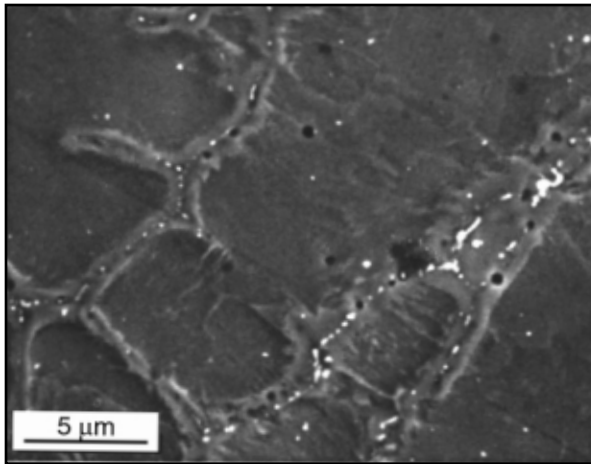


Fig. 3 — SEM micrograph showing at higher magnification the dendritic region near the tin-quenched solidification front of the Custom 450 weld.

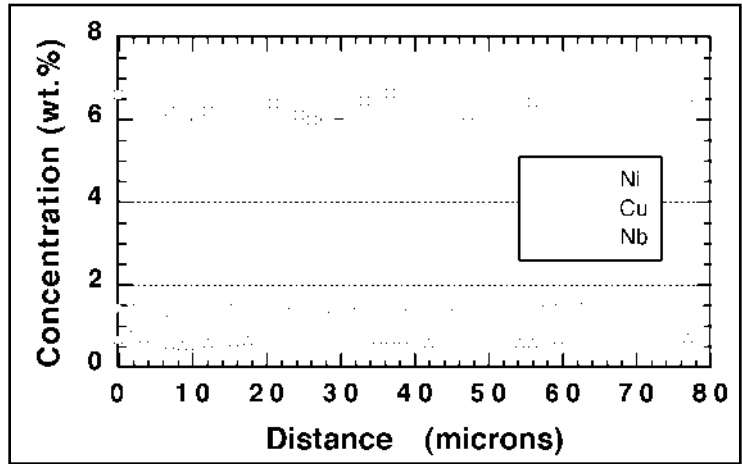


Fig. 4 — Microprobe analysis taken across the dendrite structure ~400 microns from the solidification front of the sample shown in Fig. 1.

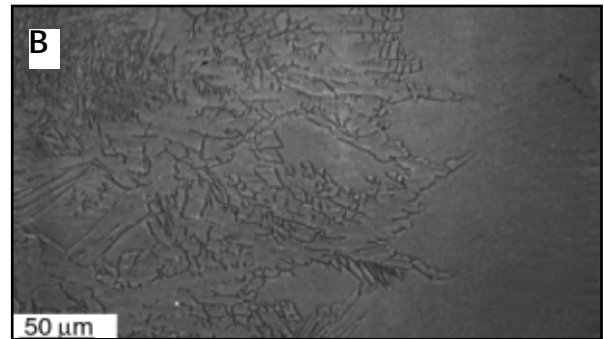
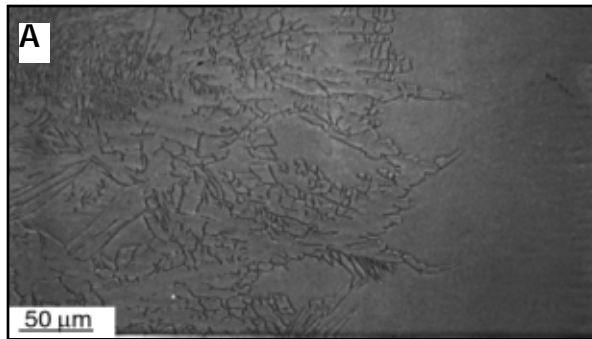


Fig. 5 — A — Solidification structure near the weld pool (to the right) of a liquid tin-quenched PH 13-8 Mo GTA weld showing evidence of alloy segregation; B — region of the decomposition of ferrite to austenite ~1 mm from the solidification front.

boundary = 2.6 wt-%; and Al core = 1.2 wt-% and boundary = 1.4 wt-%. However, it can be seen in this sample the very tips of the solidifying dendrites have not been captured. Thus, it must be expected that, as a result of some solid-state diffusion occurring during solidification, the concentrations measured at the dendrite cores are somewhat higher than what would exist at the dendrite tips. Therefore, the initial partitioning coefficients shown for PH 13-8 in Table 3 are likely somewhat high.

The region of the solid-state transformation of ferrite to austenite is shown in Fig. 5B ~1000 microns (~0.039 in.) from the weld front. Note that in the region of the quenched ferrite no evidence of segregation exists. Similar to Custom 450, homogenization of the PH 13-8 welds also occurred during solidification and cooling. As a result of elemental partitioning during the ferrite-to-austenite transformation, a small amount of ferrite is retained along the Widmanstätten austenite boundaries. In this weld, the ferrite fraction appeared to be 1–2%.

### Discussion of Microstructure Evolution

In Custom 450, as well as the other two alloys studied, little evidence of microsegregation exists in the room-temperature weld microstructures. Thus, one may have expected that partitioning coefficients could be close to 1. However, in the tin-quenched samples it was found a high degree of alloy partitioning does occur during solidification. The experimentally measured partitioning coefficients shown in Table 3 vary from ~0.85 for Ni to ~0.36 for Nb. It is evident during solidification and cooling, even at the fairly rapid cooling rates of welding, a large degree of homogenization can occur. This observed behavior is in agreement with the weld solidification model developed by Brooks and Baskes (Ref. 7) in which they incorporated solid-state diffusion. In their models, they showed, for example, that Nb in Fe, with a partitioning coefficient of ~0.25, rapidly diffuses during weld solidification, resulting in a nearly homogeneous composition. However, more re-

cently they have shown that even in GTA welds undercooling can result in higher Nb concentrations of the dendrite tip, but this effect is diminished during further solidification and cooling as a result of solid-state diffusion (Ref. 8). It must be expected that, in the welds in this study, some tip undercooling also occurred that slightly increased the initial dendrite tip concentration above the equilibrium value for elements with partitioning coefficients less than 1.

The quenching results shown for Custom 450 and PH 13-8 provide insight to the microstructural evolution of other martensitic stainless steels. In both Custom 450 and PH 13-8, the welds solidified as single-phase ferrite with no secondary solidification of austenite. One can predict the solidification behavior of stainless steels using  $Cr_{eq}/Ni_{eq}$  ratios (Ref. 9) from a variety of diagrams, such as the WRC-1992 diagram (Ref. 10). For the composition of Custom 450 used here, the  $Cr_{eq}/Ni_{eq}$  ratio, using the WRC, is 1.87, above the minimum value of ~1.7 predicting solidification occurring com-



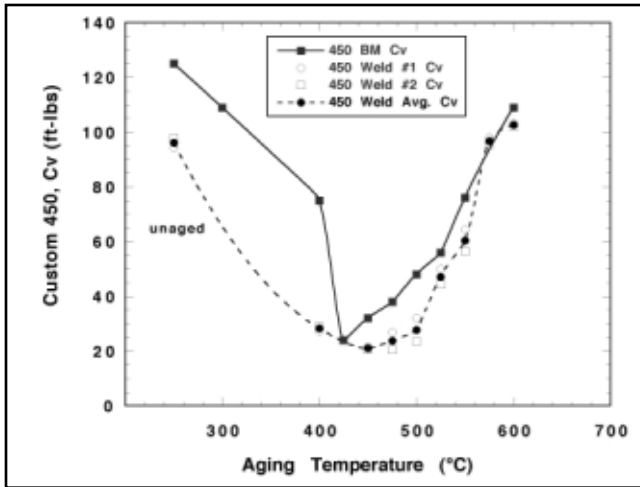


Fig. 10 — Charpy impact energies of the weld and base metals for Custom 450 in the unaged condition and as a function of aging temperature.

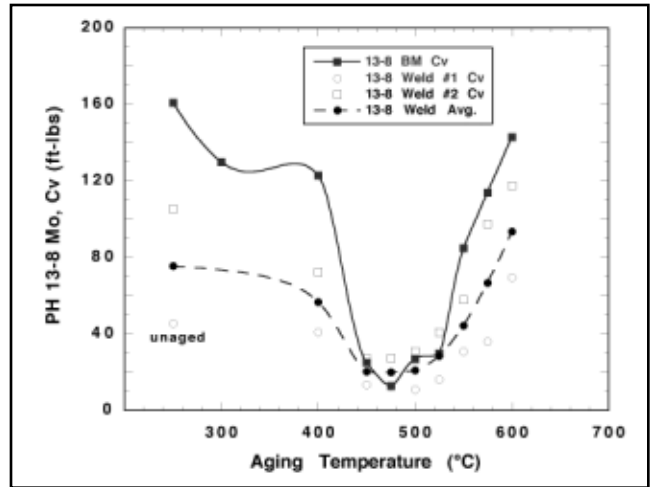


Fig. 11 — Charpy impact energies of the weld and base metals for PH 13-8 Mo in the unaged condition and as a function of aging temperature.

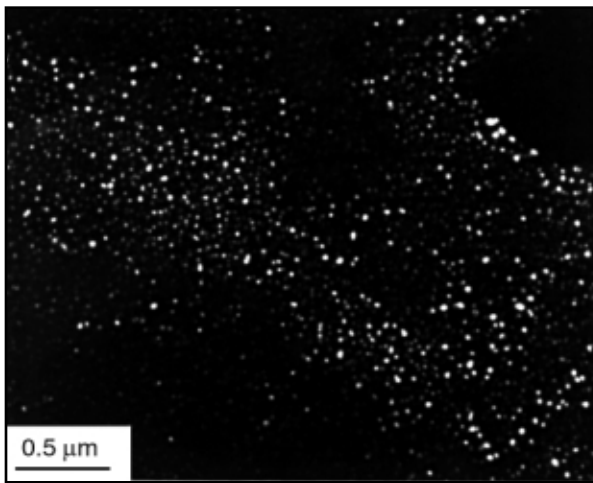


Fig. 12 — TEM dark field micrograph of PH 13-8 Mo weld fusion zone aged for 3.2 h at 550°C showing distribution of NiAl.

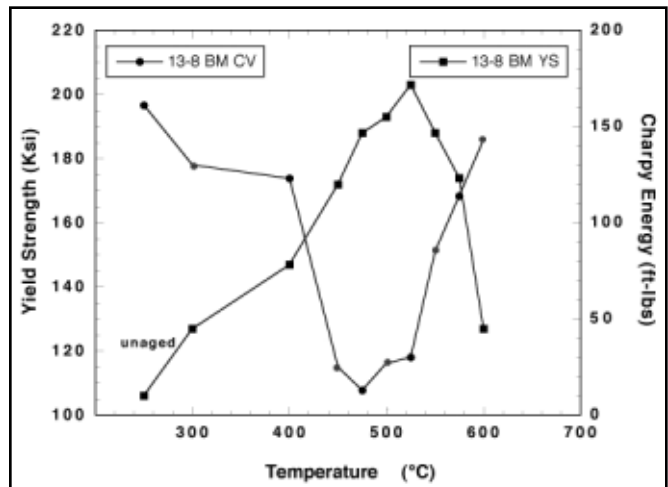


Fig. 13 — Charpy impact energy and yield strength of PH 13-8 Mo base metal plotted as a function of aging temperature.

properties for which aging times of up to 100 h were studied (1, 3.2, 10, 32 and 100 h). The 3.2 h is close to the conventional aging time of 4 h for these materials. The tensile data reported are the averages of two tests in which the variation in the two test results were typically within several ksi for both the welds and base metals. The weld tensile yield strengths are shown in Fig. 6. The aging response of the welds of all alloys is similar in that the yield strength reaches a maximum at intermediate aging temperatures and then decreases with further increases in aging temperature. Peak yield strengths for the 3.2-h age were about 195 ksi for PH 13-8 and about 180 ksi for Custom 450 and 15-5 PH. The peak strengths of Custom 450 and 15-5 PH are reached at an aging temperature

50–75°C less than the aging temperature at which the peak yield strength was achieved for PH 13-8, ~450 vs. 525°C (842 vs. 977°F).

The yield strengths of the weld and base metal of the three alloys studied are plotted in Figs. 7–9 as a function of aging temperature. In all the alloys, the nature of the aging response is similar, though varying slightly in detail. Therefore, their general behavior can be discussed together. In the unaged condition, the welds have a higher yield strength than the base metals. This trend also exists for the lower aging temperatures, with the peak strengths of the welds and base metals being very similar. Except for 15-5 PH, the peak strength of the welds is reached at an aging temperature ~50°C lower than that of the base metals. For

aging temperatures greater than that producing peak strength, the base metal of both Custom 450 and PH 13-8 has slightly higher strengths than the weld metal. However, in all three alloy systems the welds have a higher strength than the base metal when aged at 600°C (1112°F). Thus, the results suggest that weld microstructures age harden more intensely at lower aging temperatures and the weld microstructures overage more slowly than the base metals.

The Charpy impact energies of Custom 450 and PH 13-8 welds and base metals were determined for the unaged conditions and as a function of aging temperature for an aging time of 3.2 h. As shown in Fig. 10, the Charpy impact energy of the Custom 450 base metal is







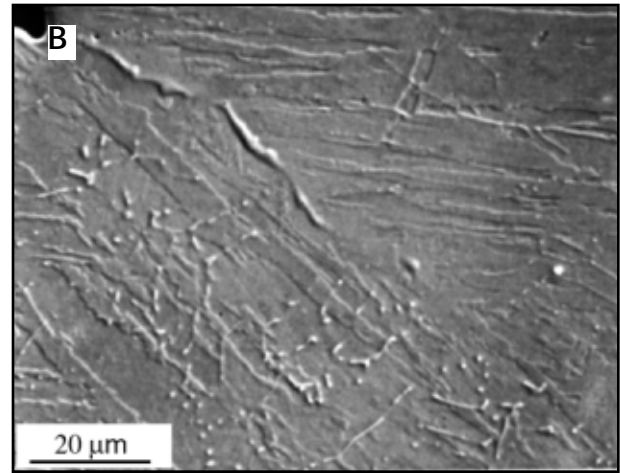
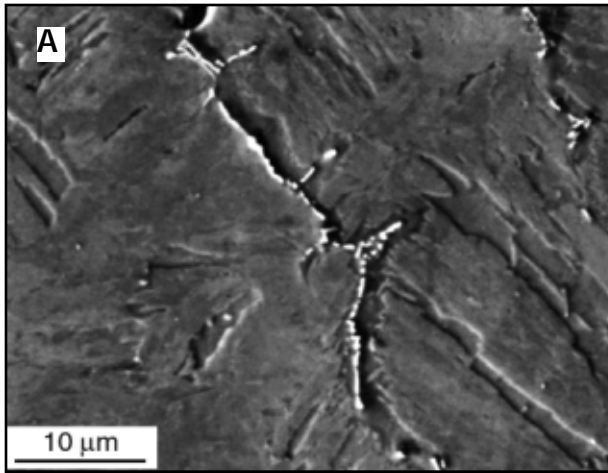


Fig. 20 — A — Solidification crack tips region of a Custom 450 Varestraint sample showing second phases associated with cracking (15-5 PH exhibited very similar appearance); B — solidification crack tip region of PH 13-8 Mo Varestraint sample.

at 475°C is shown in Fig. 16A. The fractograph indicates vertical striations associated with the long columnar grains observed in Fig. 15. This fracture surface is seen in higher magnification in Fig. 16B. These fractures exhibit a cleavage fracture mode with cleavage facets both parallel and perpendicular to the macroscopic fracture surface. The facets tend to have their longest dimension parallel to the columnar grains. If the cleavage facets are [100] planes, as is often observed in b.c.c. materials, the fractographs are consistent with the columnar grains having a [100] growth direction. For comparison, the fracture surface of Custom 450 base metal aged at 475°C (887°F) is shown in Fig. 17A. The fracture surface consists of both quasi-cleavage and microvoid coalescence, with cleavage facets 10–20 microns in dimension. The fracture surface of Custom 450 base metal aged at 450°C for 100 h, which resulted in a Charpy impact energy of about 8 ft-lb, is shown in Fig. 17B. The cleavage facets are more easily recognized on this fracture surface, but, again, they have dimensions of about 10 to 20 microns. Therefore, it is suggested that the lower toughness of the weld metal, particularly for aging temperatures of 450 through 500°C (842–1022°F) are strongly influenced by large and oriented grains, which promote cleavage fracture. However, after aging at 400°C (752°F), the strength of the weld metal is considerably greater than the strength of the base metal, as discussed previously. It is believed that the onset of the embrittlement at this temperature is primarily due to the precipitation of shearable particles.

In comparing the Charpy impact energies of the PH 13-8 weld and base

metal, there are a number of points of interest. Again, the Charpy impact energies of the welds are less than the impact energy of the base metal for the unaged and aged (at 400°C) conditions. Microstructural factors that could lead to the weld metal having lower toughness than the base metal for the unaged condition and after aging at 400°C would be the same as those presented in the discussion of the toughness of Custom 450. However, it is not clear why one of the PH 13-8 welds had much higher toughness than the other, although it is believed to be due to microstructural differences introduced by welding. It is possible that there were slight undetected variations in the welding procedure between the two plates. The effects of different thermal cycles and interpass temperature of the multiple pass welds on the aging response, austenite reversion, carbide precipitation, etc., can be very complex in determining the final weld microstructure. More work is needed to determine the sensitivity of weld process variables on weld properties.

As shown in Fig. 14, the welds of PH 13-8 are not characterized by the long columnar grains observed for Custom 450. For PH 13-8, the regions associated with each weld pass appear to be clearly delineated and large columnar grains do not appear to continue past these boundaries, as they did in the Custom 450 welds. The interfaces between weld passes appear to be important to the fracture process. As shown in Fig. 18, the crack advancing from the base of the notch appears to interact strongly with these interfaces, and these interfaces are associated with secondary cracks — perpendicular to the fracture surface — exhibiting a ductile fracture mode. The

energy absorbed by the secondary cracking processes could strongly influence the Charpy impact energy. These secondary cracks were not observed on the fracture surfaces of the Custom 450 welds that were examined. Given the high aluminum content of PH 13-8, the possibility exists that the particles at the interfaces between the weld passes in the PH 13-8 welds, which lead to the ductile secondary cracking along these interfaces, are aluminum oxide and aluminum nitride particles.

### Solidification Cracking Susceptibility

Weld solidification cracks may form during the final stages of solidification if sufficient stress or strain occurs to fracture the solidifying structure. Cracking occurs primarily along grain boundaries containing low-melting liquids. The weld solidification cracking susceptibility of Custom 450, PH 13-8 and 15-5 PH was evaluated using sub-size Varestraint testing (Refs. 6, 21). The test results, plotted as total fusion zone crack length vs. augmented strain, are shown in Fig. 19. For comparison, results from two heats of 304L, one that solidified as primary ferrite, 304L-F, with a measured ferrite number FN = 4.5, and the other that solidified as primary austenite, 304L-A with FN ~ 1, are also plotted. The Varestraint test results show that PH 13-8 is extremely resistant to solidification cracking; no cracking occurred at applied strains less than 2%, comparable to that of primary ferrite solidified 304L. Custom 450 and 15-5 PH exhibited similar cracking behavior and were more crack susceptible than PH 13-8. However, the behavior of the two alloys was much closer to the heat



The alloys Custom 450 and 15-5 PH are more crack susceptible than the alloy PH 13-8, even though all three alloys solidified as single-phase ferrite. In these alloys, the examination of Varestraint samples (Fig. 19A) shows the second phases present that can be related to cracking. However, the tin-quenched welds (Fig. 3) further show the high degree of alloy partitioning of a number of elements; the welds also show the degree of microsegregation occurring, which leads to the formation of low-melting liquid. These results would suggest the synergistic effects of a number of elements, though the examination of Varestraint samples may simply suggest the segregation of a Nb-containing liquid solidifying by a eutectic reaction involving NbC. It can also be expected that the elements Si and P may have further suppressed the temperature of final eutectic solidification.

The maximum crack lengths of the Varestraint tests are related to the temperature range of the cracking susceptible region and the thermal gradient in the region in which the crack forms. Since the low-temperature solidification reactions are similar for Custom 450 and 15-5 PH, it is not surprising that the maximum crack lengths of the two alloys are also similar. They are also much greater than those in PH-13-8 Mo, in which no significant secondary solidification reactions were observed.

## Summary

The evolution of weld solidification behavior and microstructure development was clearly revealed using tin-quenching techniques. All three alloys were shown to solidify completely as ferrite, even though some existing diagrams predict that PH 13-8 would solidify as primary ferrite with some secondary solidification of austenite. A high degree of alloy partitioning occurs during solidification, but the welds are almost completely homogenized during further solidification and cooling.

The strength and Charpy impact properties of the weld and base metals were qualitatively similar for the aging conditions studied. This similarity in the properties of the base metals and the welds was attributed to homogenization occurring during solidification and cooling, which leads to very similar microstructure and precipitate distribution. However, there were systematic differences between the aging responses of the weld and base metals; in particular, the welds had, at lower aging temperatures, a stronger aging response than did the base metals. In addition, the toughness of the

welds exhibited an embrittlement at lower aging temperatures than did the base metal.

Custom 450 and 15-5 PH would appear from Varestraint tests to be fairly resistant to solidification cracking. In these tests, PH 13-8 was shown to be extremely resistant to solidification cracking. The tin-quenched welds revealed the nature of microsegregation and structure characteristic of the state in which solidification cracking occurs. Cracking of both Custom 450 and 15-5 PH was attributed primarily to the segregation of Nb and the formation of a low-melting liquid, resulting in the eutectic solidification involving NbC. Segregation of Si and Mo may further promote cracking susceptibility.

## Acknowledgments

The microprobe analysis by P. Hlava and N. Yang, metallography by A. D. Gardia and laboratory support by J. S. Krafcik, all of Sandia National Laboratories, are greatly appreciated. This work was supported by the U. S. Department of Energy under Contract Number DE-AC04-76DP00789.

## References

- Pollard, B. 1993. Selection of wrought precipitation-hardening stainless steels. *ASM Handbook* 6: 482-494.
- Pickering, F. B. 1963. Iron and Steel Institute, Pub. 114, London, U.K., p. 131.
- Haudin, J. M., and Montheillet, F. 1978. Study by electron-microscope of hardening precipitation in delta ferrite of a stainless-steel (15%Cr,7%Ni, 2%MO): evidence of R-phase precipitation. *Metallography* 11(4): 391-438.
- Pickering, F. B. 1978. *The Physical Metallurgy and the Design of Steels*, Applied Science Publishers Ltd., London, U.K., p. 177.
- Garrison, Jr., W. M., and Brooks, J. A. 1991. The thermal and mechanical stability of austenite in the low carbon martensitic steel PH 13-8. *Mater. Sci. Eng.* A149: 65-72.
- Campbell, R. D., and Walsh, D. W. 1993. Weldability testing. *ASM Handbook* 6, 603-613.
- Brooks, J. A., and Baskes, M. I. 1986. Weld microsegregation characterization and modeling. Conference on Trends in Welding Research. *Advances in Welding Science and Technology*, ed. S. A. David, ASM International, Materials Park, Ohio, pp. 93-99.
- Brooks, J. A., Li, M., Baskes, M. I., and Yang, N. C. Y. 1997. Roles of dendrite tip undercooling and solid state diffusion on weld microsegregation. *Science and Tech of Weld. and Joining* 2(4): 160-166.
- Olson, D. L. 1985. Prediction of austenitic weld metal microstructure and properties. *Welding Journal* 64(10): 281-s to 295-s.
- Kotecki, D., and Siewert, T. A. 1992. WRC constitution diagram for stainless-steel weld metals: a modification of the WRC-1988 diagram. *Welding Journal* 71(5): 171-s to 179-s.
- Cieslak, M. J., Hills, C. R., Hlava, P. F., and David, S. A. 1990. An investigation of the high temperature and solidification microstructures of PH 13-8 Mo stainless steel. *Metall. Trans. A*, 21A: 2465-2475.
- Massalski, T. B. 1970. *Phase Transformations*, ASM International, Materials Park, Ohio, pp. 433-486.
- Brooks, J. A., Baskes, M. I., and Greulich, F. A. 1991. Solidification modeling and solid state transformations in high energy density welds. *Metall. Trans. A* 22A: 915-925.
- Elmer, J. W., Allen, S. M., and Eager, T. W. 1989. Microstructural development during solidification of stainless steel alloys. *Metall. Trans. A* 20A: 2117-2131.
- Summers, L. T., and Morris, Jr., J. W. 1985. Improvements in the Weldability of a Superconductor Sheath Material, Lawrence Livermore National Laboratory, UCRL-92346.
- Brooks, J. A. 1991. The role of solidification and microsegregation on weld performance — austenitic vs. martensitic PH stainless steels. *The Metal Science of Joining*, eds. M. Ceislak, J. Perepezko, K. Kang and M. Glicksman, pp. 107-113. TMS, Warrendale, Pa.
- Hochanadel, P. W., Robino, C. V., Edwards, G. R., and Cieslak, M. J. 1994. Heat treatment of investment cast PH 13-8 Mo stainless steel: Part 1, mechanical properties and microstructure. *Metall. Trans. A* 25: 789-798.
- Taillard, R., and Pineau, A. 1982. *Mater. Sci. Eng.* 54: 209.
- Wojcieszynski, A. L. 1993. Particle spacing and grain size effects, Ph.D. thesis, Carnegie-Mellon University, Pittsburgh, Pa.
- Hale, G. E., and Nutting, J. 1984. *International Metals Reviews* 29: 273-298.
- Lundin, C. W., Lingenfelter, A. C., Grotke, G. E., and Lessmann, G. G. 1982. The Varestraint test. *Welding Research Council Bulletin*, No. 280.
- Thier, H. 1976. *DVS-Ber.* 41:100-104.
- Brooks, J. A., and Thompson, A. W. 1991. Microstructural development and solidification cracking susceptibility of austenitic stainless steel. *International Materials Review* 36(1): 16-44.
- Lippold, J. C. 1982. Weld cracking mechanisms in austenitic stainless steels. *Trends in Welding Research in the United States*, ASM Conference Proceedings, ed. S. David, Materials Park, Ohio, pp. 209-241.
- Kujanpaa, V. P., David, S. A., and White, C. L. 1986. Formation of hot cracks in austenitic stainless steel welds. *Welding Journal* 65(8): 202-s to 212-s.
- Brooks, J. A., Thompson, A. W., and Williams, J. C. 1984. A fundamental study on the beneficial effects of delta ferrite in reducing weld cracking. *Welding Journal* 63: 71-s to 83-s.
- Lundin, C. D., Lee, C. H., and Menon, R. 1988. Hot ductility and weldability of free machining austenitic stainless steel. *Welding Journal* 67(6): 119-s to 130-s.
- Kujanpaa, V., Suutala, N., Takalo, T., and Moisio, T. 1979. Correlation between solidification cracking and microstructure in austenitic and austenitic-ferritic stainless steel welds. *Welding Research International* 9(2): 55-75.